Karshi Multidisciplinary International Scientific Journal

www.kmisj.reapress.com

K. Multidiscip. Int. Sci. J. Vol. 3, No. 3 (2026) 225–232.

Paper Type: Original Article

Electromechanical Active Suppression of Resonant Vibrations of a Six-Degree-of-Freedom Rigid Body on Viscoelastic Supports

Nuriddin Kurbonovich Esanov*

Associate Professor at the Asian International University; esanovnuriddin06@gmail.com.

Citation:

Received: 08 November 2025 *Revised: 14 February 2026* *Accepted: 22 May 2026*	Esanov, N. K. (2026). Electromechanical active suppression of resonant vibrations of a six-degree-of-freedom rigid body on viscoelastic supports. *Karshi Multidisciplinary International Scientific Journal,* 3(3), 225-232.

Abstract

This study develops a journal-style coupled electromechanical model for active suppression of resonant oscillations of a rigid body supported by viscoelastic elements. The mechanical subsystem is described by six generalized coordinates, comprising three translations and three small rotations. The support deformations are mapped to elastic and viscous reactions, while electromechanical actuators are introduced through an electrical circuit equation, back electromotive force, current-to-force conversion, and displacement–velocity feedback. The resulting formulation couples the mechanical and electrical domains and enables simultaneous modification of effective damping and stiffness. A reduced frequency-domain model is used to quantify resonance attenuation for three actuator time constants, and a six-coordinate transient calculation is performed using the parameter set provided in the source material. At the passive resonance frequency $\omega = 1.1\frac{\text{rad}}{\text{s}}$, the passive amplitude equals 5.00. Depending on the active tuning, the amplitude is reduced by approximately 67–93%; however, aggressive damping with low effective stiffness may amplify the quasi-static response. The balanced active branch $(k_{\text{eff}} = 1.05)$ limits low-frequency amplification while suppressing the passive resonance by about 67.0%, 71.2%, and 74.5% for $T = 0.01,\ T = 1,\ T = 10$, respectively. The results show that resonance attenuation and resonance-frequency management should be treated as a coupled tuning problem rather than as damping maximization alone.

Keywords: Active vibration control, Viscoelastic support, Six-degree-of-freedom rigid body, Electromechanical actuator, Resonance suppression, Frequency response, Coupled dynamics.

1 | Introduction

Rigid bodies mounted on compliant supports are encountered in machine foundations, precision platforms, transport systems, rotating equipment, and vibration-isolated technological units [1], [2]. In these systems, passive elastic and viscous elements can provide acceptable attenuation away from resonance, but their

Corresponding Author: esanovnuriddin06@gmail.com

https://doi.org/10.22105/kmisj.vi.131

Licensee System Analytics. This article is an open access article distributed under the terms and conditions of the Creative Commons Attribution (CC BY) license (http://creativecommons.org/licenses/by/4.0).

performance is limited when the excitation frequency approaches a natural frequency. The limitation is especially important for multi-axis systems because translational and rotational motions are coupled through the geometry of the support locations [3–5].

Active vibration control offers an additional mechanism for modifying the dynamic response. A practical electromechanical actuator is not an ideal force source: The generated mechanical force follows from voltage, current, electrical resistance and inductance, back electromotive force, and the actuator force constant. Therefore, a mechanically complete model should retain the electrical dynamics when the actuator bandwidth or time constant is comparable with the vibration time scale [6].

The contribution of this work is a unified six-degree-of-freedom formulation in which three translations and three rotations of the rigid body are coupled to viscoelastic support forces and electromechanical actuator dynamics [7]. The framework distinguishes two control effects: active damping, which primarily reduces the resonance peak, and active stiffness, which shifts the resonance location. This distinction is used to interpret the numerical frequency-response results and to identify a tradeoff between resonance attenuation and low-frequency amplification [8], [9].

The objective is to: 1) formulate the six-degree-of-freedom mechanical equations, 2) couple them with the actuator electrical equations, 3) obtain a frequency-domain representation suitable for resonance analysis, and 4) quantify the influence of active stiffness, active damping, and actuator time constant using the parameter sets supplied in the source document [10–12].

2 | Problem Statement and Methodology for Solving It

2.1 | Mechanical Model of the Supported Rigid Body

Let the generalized coordinate vector of the rigid body be

$$\mathrm{q}(\mathrm{t}) = \left[\xi_0(\mathrm{t}), \eta_0(\mathrm{t}), \zeta_0(\mathrm{t}), \theta_0(\mathrm{t}), \psi_0(\mathrm{t}), \varphi_0(\mathrm{t})\right]^{\mathrm{T}},$$

where ξ_0, η_0 and ζ_0 are translations of the mass center along the global x, y and z axes, while θ, ψ, and φ are small rotations. For a support point with position vector $\mathrm{r} = [\mathrm{x}, \mathrm{y}, \mathrm{z}]^{\mathrm{T}}$ relative to the mass center, the small-displacement kinematics produce linear contributions from both translation and rotation. Consequently, the local support deformation can be written compactly as $\Delta = \mathrm{Hq} - \mathrm{q_b}$, where H is a geometry matrix and $\mathrm{q_b}$ denotes prescribed base motion.

For a stationary base, $\mathrm{q_b} = 0$. Each viscoelastic support contributes a reaction consisting of an elastic and a viscous term. After assembly over all supports, the mechanical equations take the standard matrix form

$$\mathrm{M}\ddot{\mathrm{q}}(\mathrm{t}) + \mathrm{C}\dot{\mathrm{q}}(\mathrm{t}) + \mathrm{Kq}(\mathrm{t}) = \mathrm{Q}(\mathrm{t}) + \mathrm{B_f}\mathrm{F}^{\mathrm{em}}(\mathrm{t}),$$

where M is the mass–inertia matrix, C is the assembled viscous damping matrix, K is the assembled elastic stiffness matrix, $\mathrm{Q}(\mathrm{t})$ contains external generalized forces and moments, and $\mathrm{B_f}$ distributes the actuator forces into the six generalized coordinates. The off-diagonal terms of M, C and K represent translation–rotation coupling produced by product moments of inertia and non-colocated supports.

2.2 | Harmonic Excitation and Dynamic Stiffness

For harmonic loading $\mathrm{Q}(\mathrm{t}) = \mathrm{Re}\left\{\hat{\mathrm{Q}}\mathrm{e}^{\mathrm{i}\omega\mathrm{t}}\right\}$ and a steady-state response $\mathrm{q}(\mathrm{t}) = \mathrm{Re}\left\{\hat{\mathrm{q}}\mathrm{e}^{\mathrm{i}\omega\mathrm{t}}\right\}$, the passive mechanical system becomes $\left(\mathrm{K} - \omega^2\mathrm{M} + \mathrm{i}\omega\mathrm{C}\right)\hat{\mathrm{q}} = \hat{\mathrm{Q}}.$. The complex matrix in brackets is the dynamic stiffness. Resonance occurs when its determinant approaches zero and damping is insufficient to limit the response. For a scalar

equivalent mode, the amplitude relation reduces to $A(\omega) = \frac{F_0}{\sqrt{\left(k_{eff} - m\omega^2\right)^2 + \left(c_{eff}\omega\right)^2}}$. This reduced expression is used below only as a transparent resonance indicator; the full physical system remains a six-coordinate model.

2.3 | Electromechanical Actuator and Feedback Law

The electromechanical actuator is represented by an electrical circuit with inductance L, resistance R_e, and a back-EMF term proportional to the support velocity. For one actuator channel, $L\dot{I}(t) + R_e I(t) + \beta\dot{\Delta}(t) = V(t)$, where I is actuator current, β is the back-EMF coefficient, and V is the applied control voltage. The mechanical actuator force is

$$F^{em}(t) = \alpha I(t),$$

with α denoting the current-to-force coefficient. The feedback law is chosen as $V(t) = -g_p\Delta(t) - g_d\dot{\Delta}(t)$ where g_p and g_d are displacement and velocity feedback gains. In physical terms, the proportional term modifies the effective stiffness, whereas the derivative term adds active damping. The coupled model therefore captures the bidirectional interaction "mechanical motion → back EMF → electrical current" and "electrical current → actuator force → mechanical motion".

2.4 | Coupled State Representation

With multiple actuator channels, the coupled equations can be represented as

$$M\ddot{q} + C\dot{q} + Kq - B_f\alpha i = Q(t),$$
$$L\dot{i} + R_e i + \beta H\dot{q} = -G_p Hq - G_d H\dot{q},$$

where i is the actuator-current vector and G_p and G_d are feedback-gain matrices. This structure is suitable for direct time integration, eigenvalue analysis, and frequency-response calculations. It also makes explicit that an actual actuator force is filtered by the electrical dynamics rather than being generated instantaneously.

2.5 | Numerical Setup

Two parameter groups from the source material are used. The first is a normalized equivalent-mode model designed to reproduce the passive and active amplitude–frequency curves. The second is a physical six-degree-of-freedom parameter set for the rigid body and actuator. The numerical results below are therefore model-based calculations derived from the supplied parameter sets; no experimental measurements are claimed.

Table 1. Physical six-degree-of-freedom and actuator parameters used in the model.

Parameter	Value	Unit
Rigid-body mass, M	100	kg
Principal inertias, J_x; J_y; J_z	22; 24; 30	kg·m²
Products of inertia, J_{xy}; J_{xz}; J_{yz}	0.40; 0.30; 0.35	kg·m²
Supports per direction, n_1; n_2; n_3	3; 3; 3	-
Support stiffnesses, $\tilde{k}_i$; $\tilde{k}_j$; $\tilde{k}_k$	4.0×10^4; 3.8×10^4; 4.5×10^4	N/m
Support damping, $\tilde{c}_i$; $\tilde{c}_j$; $\tilde{c}_k$	400; 380; 420	N·s/m
Harmonic-force amplitude, F_0	1200	N
Actuator inductance, L	0.40	H
Electrical resistance, R_e	6.0	Ω
Back-EMF coefficient, β	12	V·s/m
Force coefficient, α	25	N/A
Feedback gains, g_p; g_d	250; 900	V/m; V·s/m

For the normalized frequency-response study, m = 1, F_0 = 1.21, k = 1.21, and c = 0.22 in the passive case, giving a resonance near ω = 1.1 rad/s and a peak amplitude close to 5. Active cases are represented by the effective stiffness and damping pairs listed in *Table 2*. The actuator time constant T is treated as a tuning parameter that changes the equivalent active damping observed in the reduced frequency-domain model.

Table 2. Effective stiffness and damping values for the reduced active-control study.

T	Active Branch	k_{eff}	c_{eff}
0.01	2	0.22	0.65
0.01	3	0.60	0.70
0.01	4	1.05	0.65
1	2	0.22	0.95
1	3	0.60	0.80
1	4	1.05	0.75
10	2	0.22	3.00
10	3	0.60	2.20
10	4	1.05	0.85

3 | Results

3.1 | Resonance Attenuation in the Frequency Domain

Fig. 1 compares the passive response with the three active branches for T = 1. The passive curve has a narrow resonance near ω = 1.1 rad/s. All active branches suppress this resonance, but they do so with different low-frequency penalties. Branch 2 provides the strongest suppression around the passive resonance but has a small effective stiffness, so its static amplitude $A(0)=\frac{F_0}{k_{eff}}=5.5$ reaches 5.5. Branch 4 retains a much larger effective stiffness and therefore gives a more balanced response over the full frequency range.

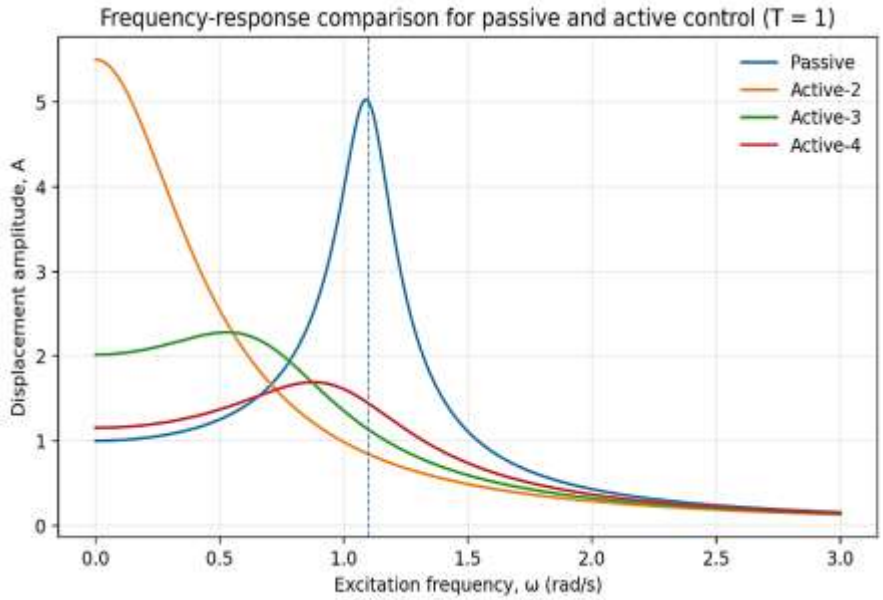


Fig. 1. Frequency-response curves of the equivalent mode for the passive system and three active-control branches at T = 1.

Table 3. Quantitative resonance indicators calculated from the supplied effective parameters.

Case	T	Keff	Ceff	ω peak	Apeak	A(1.1)	Reduction at 1.1 (%)
Passive	-	1.21	0.22	1.089	5.025	5.000	0.0
Active 2	0.01	0.22	0.65	0.093	5.504	0.991	80.2
Active 3	0.01	0.60	0.70	0.596	2.502	1.232	75.4
Active 4	0.01	1.05	0.65	0.916	1.916	1.651	67.0
Active 2	1	0.22	0.95	0.000	5.500	0.841	83.2
Active 3	1	0.60	0.80	0.529	2.280	1.130	77.4
Active 4	1	1.05	0.75	0.877	1.692	1.440	71.2
Active 2	10	0.22	3.00	0.000	5.500	0.351	93.0
Active 3	10	0.60	2.20	0.000	2.017	0.485	90.3
Active 4	10	1.05	0.85	0.830	1.527	1.276	74.5

The passive amplitude at ω = 1.1 rad/s is exactly 5.00 for the selected normalized parameters. At the same frequency, branch 2 reduces the amplitude to 0.991, 0.841, and 0.351 for T = 0.01, 1, and 10, corresponding to reductions of 80.2%, 83.2%, and 93.0%. Branch 3 gives reductions of 75.4%, 77.4%, and 90.3%. Branch 4 gives smaller but more uniform reductions of 67.0%, 71.2%, and 74.5%, while maintaining A(0) ≈ 1.15. These values demonstrate a practical tuning compromise: maximum damping does not automatically give the best broadband vibration isolation because effective stiffness controls the low-frequency displacement.

3.2 | Six-Coordinate Transient Decay

The source parameter set also specifies initial displacement, initial velocity, decay coefficient λ, and oscillation frequency ω for all six generalized coordinates. To provide a consistent time-domain visualization, each coordinate is reconstructed by the damped modal expression $q(t) = e^{-\lambda t}\left[C\cos(\omega t) + D\sin(\omega t)\right]$, with $C=q(0)$ and $D = \frac{\dot{q}(0) + \lambda q(0)}{\omega}$. This representation exactly satisfies the supplied initial conditions and decay/frequency parameters and is used here as a reference transient response rather than as a substitute for numerical integration of the complete coupled state-space equations.

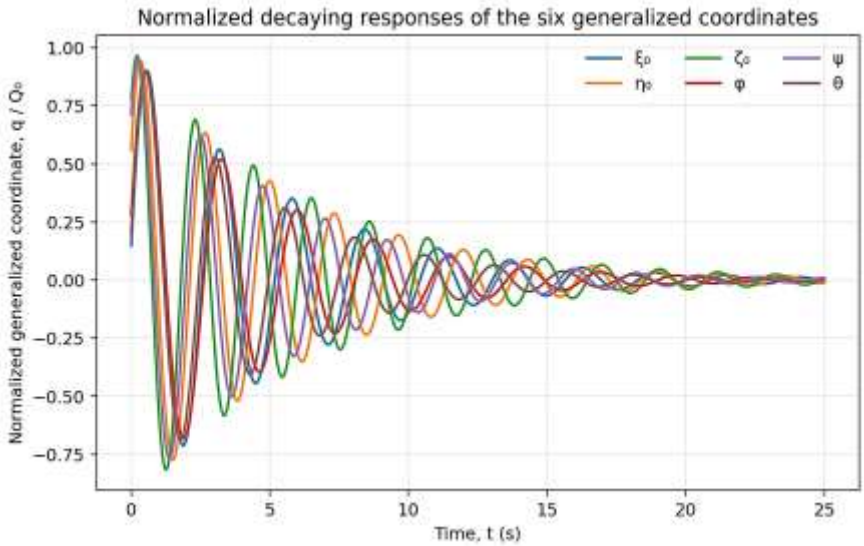


Fig. 2. Normalized transient decay of the three translational and three rotational generalized coordinates using the supplied λ and ω values.

Table 4. Initial conditions and modal-decay indicators for the six generalized coordinates.

Coordinate	q(0)	Unit	q(0)	Unit	λ (s⁻¹)	ω (rad/s)	Q_0 Envelope	2% Envelope Time (s)
ξ_0	0.0119	m	0.1890	m/s	0.18	2.40	0.0805	21.73
η_0	0.0346	m	0.1327	m/s	0.17	2.70	0.0619	23.01
ζ_0	0.0370	m	0.0843	m/s	0.16	3.00	0.0477	24.45
φ	0.0078	rad	0.0600	rad/s	0.20	2.30	0.0279	19.56
ψ	0.0148	rad	0.0382	rad/s	0.19	2.80	0.0208	20.59
θ	0.0057	rad	0.0686	rad/s	0.21	2.50	0.0285	18.63

The modal envelopes decay monotonically because all λ values are positive. The estimated time for the envelope to fall to 2% of its initial value ranges from 18.63 s for θ to 24.45 s for ζ_0. The rotational and translational coordinates therefore exhibit comparable decay time scales, which is consistent with a controller that acts on both force and moment channels. The largest initial modal envelope is associated with ξ_0, whereas the slowest envelope decay is obtained for ζ_0 because it has the smallest decay coefficient, $\lambda = 0.16\ s^{-1}$.

4 | Discussion

The numerical study highlights three points relevant to the design of active vibration isolators. First, active damping primarily controls the height of the resonance peak. Increasing c_eff strongly decreases the response at the passive resonance frequency. Second, active stiffness influences both the quasi-static response and the resonance location. A controller with excessively small effective stiffness can produce excellent resonance suppression while allowing a large low-frequency displacement; this behavior is visible for active branch 2. Third, the actuator time constant changes the effective control action. In the supplied parameterization, larger T is associated with stronger equivalent damping for branches 2 and 3, which increases attenuation near $\omega = 1.1\ \text{rad/s}$ but also emphasizes the importance of considering electrical dynamics and phase lag.

The six-degree-of-freedom formulation is important because active forces applied away from the mass center create control moments as well as translations. A one-dimensional model cannot represent cross-axis coupling, products of inertia, or geometric lever arms of the supports. In contrast, the present matrix form can be extended directly to multiple rigid bodies, multiple support groups, non-identical actuators, and base excitation. The same formulation also enables eigenvalue placement, robust-control design, and actuator saturation constraints to be added without changing the underlying mechanical topology.

A limitation of the present draft is that the available source data contain parameter sets and analytical relationships but not experimental measurements or a complete numerical integration record of the coupled electrical–mechanical state equations. Accordingly, the reported curves are model-based calculations. For journal submission, the strongest next step would be experimental or high-fidelity finite-element validation, together with sensitivity analysis for uncertain stiffness, damping, electrical resistance, inductance, and time delay.

5 | Conclusion

I. A coupled electromechanical model was formulated for a rigid body with three translational and three rotational degrees of freedom on viscoelastic supports.

II. The actuator model explicitly retains inductance, resistance, back EMF, current-to-force conversion, and displacement–velocity feedback, making the control force dynamically realizable rather than instantaneous.

III. For the normalized passive model, the resonance amplitude at $\omega = 1.1$ rad/s equals 5.00. Active tuning reduces this amplitude by approximately 67–93% for the supplied parameter sets.

IV. Aggressive active damping with low effective stiffness can introduce large low-frequency displacement. The keff = 1.05 branch provides the most balanced broadband behavior among the three supplied active branches.

V. The six generalized coordinates exhibit decaying transient envelopes with 2% envelope times of approximately 18.6–24.5 s for the supplied λ values.

VI. The model provides a suitable basis for optimization of controller gains, actuator bandwidth, and support geometry, but experimental or high-fidelity numerical validation is required before engineering deployment.

Acknowledgments

In this article, the author contributed equally, and the author jointly developed the ideas and achieved the results through collaborative thinking.

Author Contributaion

In this article, all authors contributed equally, and the authors jointly developed the ideas and achieved the results through collaborative thinking.

Funding

This section indicates any support that is not included in the Author Contribution or Funding sections. Such support may include administrative and technical support or in-kind donations (e.g., materials used for experiments).

Data Availability

Data available on request due to ethical reasons.

Conflicts of Interest

The author declares that he has no conflict of interest. "Funders played no role in the design of the study, in the collection, analysis, or interpretation of the data, in the writing of the manuscript, or in the decision to publish the results."

Consent for Publication

The author confirms consent for the publication of this work.

Ethics Approval and Consent to Participate

This article does not contain any studies with human participants performed by the author.

References

[1] Inman, D. J. (2014). *Engineering vibration*. Pearson. https://www.pearson.com/en-gb/subject-catalog/p/engineering-vibrations-international-edition/P200000004530/9780273768449?

[2] Rao, S. S. (2017). *Mechanical vibrations*. Pearson. https://www.pearson.com/en-gb/subject-catalog/p/Rao-Mechanical-Vibrations-in-SI-Units-6th-Edition/P200000005274?

[3] Meirovitch, L. (1990). *Dynamics and control of structures.* Wiley. https://www.wiley-vch.de/en/areas-interest/engineering/dynamics-and-control-of-structures-978-0-471-62858-3?

[4] Preumont, A. (2011). *Vibration control of active structures: An introduction*. Springer. https://doi.org/10.1007/978-94-007-2033-6

[5] Fuller, C. R., Elliott, S. J., & Nelson, P. A. (1996). *Active control of vibration*. Academic Press. https://www.sciencedirect.com/book/monograph/9780122694400/active-control-of-vibration?

[6] Ogata, K. (2010). *Modern control engineering*. Prentice Hall. https://www.pearson.com/en-us/subject-catalog/p/modern-control-engineering/P200000003521/9780136156734?

[7] Franklin, G. F., Powell, J. D., & Emami-Naeini, A. (2015). *Feedback control of dynamic systems*. Pearson. https://books.google.com/books?id=WaozngEACAAJ&utm

[8] Ruziyev, T., Safarov, I., Teshayev, M., Boltayev, Z., Esanov, N., Usmanov, B., ... & Urolov, U. (2026). Assessment of the dissipative properties of viscoelastic hollow cylindrical bodies with filler during the propagation of natural waves. *Journal of composites science*, *10*(8), 437. https://doi.org/10.3390/jcs10080437

[9] Safarov, I., Teshaev, M., Ishmamatov, M., Esanov, N., Bayaly, A., Axmedov, S., & Almuratov, S. (2026). Free and forced vibrations of structurally inhomogeneous rod mechanical systems. *Sound & vibration*, *60*(2). https://doi.org/10.59400/sv3993

[10] Yunusov, G. G., Esanov, N. Q., Almuratov, S. N., Ablokulov, S., & Sobirov, R. (2022). On numerical simulation of vibrations in radio-electronic structures. *AIP conference proceedings* (Vol. 2467, No. 1, p. 060038). AIP Publishing LLC. https://doi.org/10.1063/5.0094082

[11] Safarov, I. I., Teshaev, M. K., Boltayev, Z. I., Karimov, I. M., & Esanov, N. Q. (2023). Natural and forsed osculations of pipelines in contact with the wincler medium. *E3S web of conferences* (Vol. 411, p. 01005). EDP Sciences. https://doi.org/10.1051/e3sconf/202341101005

[12] Esanov, N., Saipnazarov, J., Almuratov, S., Raxmonova, G. Z., & Ishmamatov, M. (2025). Free vibrations of a spherical shell with a pinched edge. *AIP conference proceedings* (Vol. 3268, No. 1, p. 030008). AIP Publishing LLC. https://doi.org/10.1063/5.0258149